A hydrogel-based optical fibre fluorescent pH sensor for observing lung tumor tissue acidity

Jingjing Gong[a,b], Michael G Tanner[b,c], Seshasailam Venkateswaran[a], James M Stone[d], Yichuan Zhang[e], Mark Bradley[a,b,*]

[a]School of Chemistry, EaStCHEM, University of Edinburgh, King's Buildings, West Mains Road, Edinburgh, EH9 3FJ, UK

[b]EPSRC Proteus Hub, Centre for Inflammation Research, Queen's Medical Research Institute, University of Edinburgh, 47 Little France Crescent, Edinburgh, EH16 4TJ, UK

[c]Institute of Photonics and Quantum Sciences, School of Engineering and Physical Sciences, Heriot-Watt University, Edinburgh, EH14 4AS, UK

[d]Centre for Photonics and Photonic Materials, Department of Physics, University of Bath, Bath, BA2 7AY, UK

[e]Shenzhen Institutes of Advanced Technology, Chinese Academy of Sciences, Shenzhen, China

*Corresponding Author: Email: mark.bradley@ed.ac.uk.

Tel: 0044 131 650 4820

Address: School of Chemistry, EaStCHEM, University of Edinburgh, King's Buildings, West Mains Road, Edinburgh, EH9 3FJ, UK

Abstract

Technologies for measuring physiological parameters in vivo offer the possibility of detection of disease and its progression due to the resulting changes in tissue (pH, O_2, temperature, etc.). Here, a compact hydrogel-based optical fibre pH sensor was fabricated, in which polymer microarrays were utilized for the high-throughput discovery of the optimal matrix for pH indicator immobilization. The fabricated hydrogel-based probe responded rapidly to pH changes and demonstrated a good linear correlation within the physiological pH range (from 5.5 to 8.0) with a precision of 0.10 pH units. This miniature probe was validated by measuring pH across a whole ovine lung and allowed discrimination of tumorous and normal tissue, thus offering the potential for rapid and accurate observation of pH tissue changes.

Keywords: optical fibre; hydrogel-based pH sensor; polymer microarray; in situ photo-polymerization; lung tumor

1. Introduction

States of human health are often reflected by various physiological parameters, however deep-tissue monitoring of such parameters remains a challenge. Due to the advantages of miniaturization, flexibility, biocompatibility and real-time measurements, optical fibre-based sensors have been developed to measure various physiological parameters, such as pH, O_2, NO and glucose,[1-5] and due to the properties of optical fibre itself potentially allow remote measurements within human body.

Dysregulated pH is a cancer marker, which could be exploited to help detect disease and determine its margins and help develop cancer-specific therapeutics.[6-8] Optical fibre-based pH sensors have been developed as a means of measuring pH in both single cells[9-11] (showing that extracellular pH (pH_e) of tumor cells is lower than healthy cells), and

distinguishing different tissues in human breast cancers[12] (showing a more acidic surface for the cancerous tissues compared to healthy tissues). However, there are few reports of using optical fibre pH sensors to measure lung cancer tissue acidity, in part due to the challenge of developing reliable and compact combinations of fibre and sensor. Fibre-optic chemical sensors and biosensors[13] have traditionally focused on the development of pH indicators, including the attachment of organic pH-sensitive dyes and their covalent immobilization[14-20], sensors over a wide range of pH[21-29] and the use of quantum dots[30, 31]. However, few papers have explored the effect of the immobilization matrix itself on the optical fibre sensor performance, even though, to date, the majority of optical fibre pH-based sensors have been fabricated with the indicators immobilized in polymers including hydrogels.

The polymer-microarray technique is an approach whereby hundreds or thousands of different polymer features can be fabricated on a glass slide, with subsequent parallel screening of the polymer library.[32-36] Here, the polymer-microarray approach was used to screen a hydrogel library and identify an optimal hydrogel as an ideal matrix for immobilization of the pH reporter and fabrication of the optical fibre-based pH sensor.

Thus a hydrogel-based optical fibre pH sensor was fabricated by in-situ photo-polymerization, employing a hydrogel as an immobilization matrix for the pH-indicator. The fluorophore choices (5(6)-FAM and Porphyrin) were made for a number of reasons, notably pH sensitivity, intensity and wavelength (both excitation and emission). Thus: (i). Both be excited using the same wavelength of light (simplifying the instrumental set-up and eliminating intensity variation changes that might otherwise occur); (ii). The emission and absorption spectra were such that unwanted fluorescent energy transfer would not occur between the two dyes; (iii). 5(6)-FAM is a well-known pH sensor, while the Porphyrins emission was insensitive to pH, thus offering a robust ratiometric means to measure pH; (iv). Both dyes were optically bright and optically robust. The polymer-microarray identified

hydrogels, which showed optimal dye-trapping abilities while maintaining their pH responsivity. Properties such as sensitivity, pH precision, time response and reversibility were investigated. This enabled the development of a pH sensor with good sensitivity and accuracy with a footprint of only 250 µm (glass fibre diameter) and was applied for the measurement of pH on cancerous lung tissue. With robust packaging, the compact probe would provide a promising tool for real-time pH measurements

2. Experimental

2.1 General

All monomers were purchased from Sigma Aldrich except tridecafluoro-1,1,2,2-tetrahydrooctyl-dimethylchlorosilane (FDS) (ABCR GmbH Co. KG) and NMP (99%, Alfa Aesar) from Fisher Scientific. Microscope glass slides (76 × 26 mm) was purchased from Menzel GmbH Co.KG. Glass coverslips (Φ15 mm) were purchased from Menzel-Gläser (Germany). Graded-index multimode optical fibre was fabricated by the Centre for Photonics & Photonic Materials, University of Bath, and was used in all optical sensing experiments. pH 4.0 to pH 5.5 buffers were made using potassium hydrogen phthalate (0.1 M) adjusted with hydrochloric acid or sodium hydroxide (0.1 M). pH 6.0 to pH 8.0 buffers were made by using appropriate ratios of monobasic and dibasic sodium hydrogen phosphate (0.1 M). pH 8.5 to pH 10.0 buffers were made by using sodium tetraborate (0.1 M) adjusted with hydrochloric acid or sodium hydroxide (0.1 M). The pHs' of the buffer solutions were measured using a glass-electrode pH meter (Mettler Toledo).

A Zepto O_2 plasma generator (Diener electronic GmbH, Germany) was used for slide cleaning. A Scienion S5 SciFLEXARRAYER equipped with a Piezo Dispense Capillary PDC 80 with a 50 µm aperture (Scienion AG, Germany) was used for inkjet printing. The printing dispenser (with a Type 2 coating to aid the printing of samples dissolved in non-

aqueous solvents) was washed at least once between each printing/deposition and the NMP wash station was refreshed every 20 min to prevent cross-contamination.[32]

The hydrogels were photo-polymerized using a UVPTM CL-1000 Ultraviolet Crosslinker. An Axiovert 200m inverted fluorescence microscope running the Axiovision 4.8 software (Carl Zeiss AG, Germany) was used for fluorescent imaging of the polymer microarrays and the fibre probes. Image analysis was carried out in ImageJ. The fluorescent intensities of the polymer-coated coverslips were measured with a BioTek SynergyHT plate reader. Morphological characterization of the deposited polymer films was carried out using an optical microscope (Leica Microsystems Inc., Bannockburn, 1L, USA) with a CCD camera (Hitachi model 3969, Japan) and a focused ion beam SEM (FIB/SEM) service (Zeiss Crossbeam 550). A 405 nm laser diode (CVI Melles Griot) was used for fabrication of optical fibre probe. The 485 nm laser from PicoQuant (LDH-D-C-485) was combined with a laser driver (PDL 800-D, Picoquant). Fluorescence spectra were captured on a fibre coupled spectrometer (Ocean Optics QEPro). The triggering unit (TTL pulse generator) controlled both laser and spectrometer allowing on demand integration with 100 ms synchronised measurements. All other optical components were purchased from Thorlabs.

2.2 Preparation and Screening of the Hydrogel Microarray

The inkjet mediated preparation of microarrays has been reported in detail previously[32, 33]. Hydrogel microarrays consisting of 180 different polymers were fabricated by inkjet printing on glass slides (Figure 1A). For the fabrication of microarrays, microscope glass slides (76 × 26 mm purchased from Menzel GmbH) were cleaned using an O_2 plasma prior to generation of a hydrophobic mask (tridecafluoro-1,1,2,2-tetrahydrooctyl-dimethylchlorosilane)[32, 37]. The mask drives the localization of the printed solutions (solutions of monomers, crosslinker, initiator and the fluorophore) into the unmasked circular spots. This solution is then

polymerized to create circular hydrogel spots containing the fluorophore. Briefly, arrays were fabricated by printing NMP solutions of monomers (1 M) together with N,N'-Methylenebis (acrylamide) (MBA 1 M) on a masked glass slide with over-printing of the pH sensitive probe 5(6)-carboxyfluorescein (5(6)-FAM 10 mM) and the photo-initiator diphenyl (2,4,6-trimethylbenzoyl) phosphine oxide (TPO 1 M) deposited onto each spot. The molar ratio (MBA:monomers:5(6)-FAM:TPO) was 90:360:1:20 and was kept constant for all experiments. The volumes of the printed monomer and dye solutions are ≈ 21 nL, while the droplets are rapidly released from the tip during printing, thus ensuring a homogeneous distribution across the printed features.[38, 39] The printing dispenser was washed at least once between each printing and the NMP in the wash station was refreshed every 20 min to prevent cross-contamination.

After printing the glass slides were exposed to UV irradiation (UVPTM CL-1000 Ultraviolet Crosslinker, 365 nm, 8 Watt, 1000 $mJ \cdot cm^{-2}$) for 30 mins, and then dried at 40℃ overnight. Each array had 45 × 12 spots giving 180 different polymers of each printed feature in triplicate. The image and layout of the hydrogel microarrays printed on the glass slide is shown in Table S1. The diameter of the features was ca ≈ 400 μm, and the distance between each spot was 1 mm (Figure 1B).

To identify hit hydrogels with good dye-trapping ability and pH sensitivity, the hydrogel microarray was incubated in pH 10.0 and pH 4.0 buffers for 30 mins and imaged. From the initial polymer microarray screening eight hydrogels ('hits') with the biggest fold increase in fluorescence were identified. These 'hits' were scaled-up and coated onto coverslips, repeating the same screening process in different pH buffers. After two iterative rounds of screening, 3 lead hydrogels were identified and assessed on the optical-fibre-based sensing platform.

2.3 Optical-Fibre-Based Sensing Platform

The optical-fibre-based sensing platform is shown in Fig. S1A and was based on our previous works[5, 16, 40]. The main parts of the detection system consisted of a 485 nm laser, an epi-fluorescence system, synchronised triggering from a signal generator, a spectrometer and an optical fibre probe. The excitation light (485 nm) was launched into the platform and passed through the epi-fluorescence system to couple into the optical fibre probe. Following illumination of the fluorescent dyes, light emitted from sensing probe was guided back through the epi-fluorescence system and collected by a spectrometer. The triggering system allowed short illumination times (100 ms) with synchronised measurements to decrease the total illumination exposure, reducing the effect of photo-bleaching on the fluorescent sensors. Preparation of the pH probes shared the same detection system platform, with the exception of a 405 nm laser and filter for the photo-polymerization chemistry.

2.4 Fabrication of the pH Probe

A 5 cm length of the protective coating at each end of a 1 m length of optical fibre was removed followed by cleaving each end (1 cm removed) to give a fresh flat surface. The exposed optical fibre was incubated in NaOH (1 M) overnight, and washed with water and acetone, then dipped into a 20% (v/v) solution of 3-(trimethoxysily) propyl methacrylate (TMSPMA) in acetone for 1 hour. The fibre was then washed with acetone and dried with N_2 prior to photo-polymerization. The optical fibre surface was activated by immersion in NaOH and then in TMSPMA to give an optical fibre surface tip that would react with monomers and the cross-linker (Figure 2A).

The polymerization reaction solution consisted of a homogeneous solution of the ‘lead’ monomers, MBA (the cross-linker), and TPO as a photo-initiator, and the two reporters 5(6)-FAM and 5,10,15,20-Tetrakis(4-hydroxyphenyl)-21H,23H-porphine (Porphyrin) (the dye

ratio used was 1:1). The optical fibre was irradiated at 405 nm for defined amounts of time with a N_2 flow (Fig. S1B), allowing polymer growth to proceed from the reaction solution, with the layer of hydrogel encapsulating the reporters onto the fibre tips.

2.5 Characterization of the Optical Fibre pH Sensor and Lung Tumor Measurements

All of the pH response experiments were carried out using optical fibre sensors in the dark at 25℃. All fluorescence measurements were conducted using a 485 nm laser at 1 μW (triggered on demand for 100 ms) unless otherwise noted. Assessment of the optical fibre pH sensors was conducted using a series of buffer solutions prepared between 4 to 10. The elected hydrogel system (1:1 HBMA/DMAEA named here H3) was precisely calibrated with pH buffers in the physiological relevant window (from 5.5 to 8.0). For each pH buffer measurement, 3 replicates were performed to verify the repeatability/robustness of the optical fibre sensors. By measuring the area under the curve (AUC) the ratio of 5(6)-FAM (from 510 to 630 nm) and Porphyrin (from 630 to 850 nm) (See Fig. S2), the pH of the buffers were characterized and used for calibration.

To test the reversibility of the optical fibre sensors, the immersion buffers were changed from pH 5.5 to 8.0 and back five times, and emission spectra collected after a short delay (1 min). The response time of the sensor was analyzed by transferring of the probe tip from solutions at pH 5.5 to 8.0 and back to pH 5.5 with continuous illumination at 485 nm during the whole process. Emission spectra were automatically recorded every 100 ms. For triggered measurements, the optical fibre pH sensor was washed with deionized water between each measurement, with the exception of response-time measurements, where the changes in fluorescence intensity were measured without washing and direct transfer from one buffer to another.

Ovine lungs were from ewes destined for cull and euthanized under Schedule 1 of Animals (Scientific Procedures) Act 1986. The optical fibre pH sensor was calibrated using three pH buffers (pH 5.5, 6.5 and 7.5) before each tissue measurement. Tissue measurements were obtained from 3 tumour locations and 6 healthy locations with the fabricated probes threaded inside a hollow needle, that penetrated into the sample. (Fig. S1C). Three measurements were recorded at each location, with the probe washed in water between each measurement. Following the tissue pH measurements with the optical fibre sensors, each optical probe measurement site was measured for comparison using a commercial tissue pH probe (Mettler Toledo) via a small incisions. For both the optical fibre and commercial probe, three replicates were measured.

3. Results and Discussion

3.1 Hit Hydrogels Identification by Polymer Microarray

180 features, containing monomers, cross-linker, pH sensitive dye and photo-initiator were printed one by one (each one in triplicate), following in situ photo-polymerized on the glass slide. A high-throughput screening strategy was used to identify hit polymers, which efficiently trapped the dyes and allowed pH sensing – thus the screen was for cross-linked polymers that showed good dye-trapping abilities and little evidence of the fluorophores leaching from the polymer film even though the dye molecules are only physically entrapped by the polymer.

The fluorescence intensities of the polymers entrapping the dyes were captured by fluorescence microscopy and the intensity of the features quantified with ImageJ (see Figure 1C) and the fold increases in the fluorescence of the screened polymers were analysed (see Table S2). Because of the differences in the dye-trapping abilities and proton transfer efficiency of the different hydrogels, the fluorescence intensity of each spot varied when

changing from alkaline to acidic buffers. The high-throughput assay thus enables the trapping abilities and fluorescent responsiveness of all hydrogels to be rapidly screened, with 8 'hit' hydrogels identified (highlighted in red in Table S2). The average fold increase in fluorescent intensity (when changing from pH 4.0 to pH 10.0) of the eight most highly performing polymers (from amongst all 180 features) ranged from approximately 4.5 to 16.0. These eight (so-called "hit" polymers) were observed to have a variety of chemical compositions but also some similarities: Four of these hydrogels contained monomers with amine groups (dimethylaminoethyl acrylate (DMAEA), 2-(dimethylamino)ethyl methacrylate (DMAEMA), which could be protonated at physiological pH's, thus promoting proton transport through the polymers as well as binding 5(6)-FAM via ionic interactions. In addition, most of "hit" hydrogels contained hydroxy groups (e.g. 4-hydroxybutyl methacrylate (HBMA), 2-hydroxyethyl methacrylate (HEMA) or 2-hydroxy-3-phenoxypropyl acrylate (HPPA)) that promote hydration and proton transfer.

In order to better control the polymer coating, the 8 'hits' were resynthesized onto 15 mm diameter coverslips and their dye-trapping abilities and pH responsiveness were re-assessed. Figure 3 illustrates the properties of the 8 'hits' with their respect to their dye trapping abilities and pH sensitivities. Three 'lead' polymers (1:3 HPPA/HEMA, PHPMA, 1:1 HBMA/DMAEA, abbreviated here as H1, H2, H3 respectively) were observed to display the most optimal pH sensitivities between pH 4.0 and pH 10.0 and were further assessed on the optical-fibre-based sensing platform.

3.2 Assessment of the Lead Hydrogels and Laser Adjustment

An optical-fibre-based sensing platform was developed for assessment of the performance of the 'lead' polymers in a more realistic application scenario. Detailed analysis of the response of the optical fibre pH sensors immobilized with the lead candidates (H1, H2, H3) are shown

in Fig. S3 with all of them displaying strong responsiveness to pH changes, with H3 exhibiting the greatest pH sensitivity. The emission spectrum from H3 was notably stronger and the fluorescent signals less noisy (Fig. S3C) compared to those from H1 and H2.

The fabricated optical fibre pH sensor coated with H3 demonstrated the most dynamic responsiveness across a pH range from 5.0 to 9.0 (see Fig. S3F). Considering the chemical structure of hit polymer H3, (see Figure 2B) we note it contains tertiary amine (that will be protonated at physiological pH's) and hydroxyl groups that could both be used to trap the fluorophore e.g. via ionic interactions as well as allow proton transport. In short, this study revealed the H3 system as an optimal matrix for immobilization of pH probes and fabrication of fluorescence based optical fibre pH sensors with good pH responsiveness.

In order to optimise fabrication of the optical fibre pH sensors, laser power and irradiation times were adjusted to vary the photo-polymerization of the H3 system. As shown in Fig. S4, the hydrogel films coated on the fibre tip showed an obviously dependency on laser exposure time/power. Higher laser output powers (5 mw) caused the generation/deposition of large polymer cluster (Fig. S4D), resulting in a fabricated optical fibre sensor that showed limited sensitivity to pH changes. Whereas at lower powers (1 mw), the robustness of the optical fibre pH sensor was observed to initially improve with an increase in photo-polymerization time (from 0.5 to 2 mins), due to increased levels of attachment of dyes and hydrogels onto the tip of the fibre. A deposition time of 5 min resulted in an excessively thick layer of hydrogel that slowed the sensors response to pH changes. Photo-polymerization conditions of a laser output power of 1 mw for 2 min were found here to be optimal for the fabrication of the optical fibre pH sensors.

3.3 Probe Characterization

The SEM images of the fibre tip are shown in Figure 4. The whole probe head area was observed to be coated with a layer of polymer, but upon drying the surface was neither flat nor smooth with numerous creases, perhaps expected when a hydrogel dries. Any response variations between probes were eliminated by calibration of the optical fibre pH sensors before measurement. Investigation of the hydrogel was carried out by cross-sectional cutting using a focused ion beam system (FIB/SEM). The thickness of the polymer-coating layer varied across the end of the fibre - from a few microns to dozens of microns (see Figure 4). The optical microscopy images of the sensor coated onto the tip of an optical fibre showed that the polymer film was attached onto the end of the fibre and both 5(6)-FAM and Porphyrin were trapped within the polymer film (figure 4G and H show images of the fibre tip observed through the fluorescein channel before and after pH measurements respectively). After pH measurement the hydrogel films remained attached onto the end of the fibre with strong fluorescent intensities observed under the fluorescein channel, indicating a robust optical fibre sensor.

3.4 Calibration and Characterization of the pH Probe

Figure 5 shows the emission spectra of the hydrogel-based optical fibre pH sensor. It is apparent that the fluorescence intensity of 5(6)-FAM was highly sensitive to pH. In order to eliminate the effect of the excitation source or fibre coupling fluctuations, Porphyrin was incorporated as an internal reference. The calibration lines of the ratios of the areas under the curves (AUC) (see section 2.5) versus pH were plotted and normalized between pH 5.5 to pH 8.0, as this covers the physiologically relevant pH range using the equation[14]:

$$\textit{Normalized sensor response} = \frac{AUC\ ratio_{\mathrm{pHx}} - AUC\ ratio_{\mathrm{pH5.5}}}{AUC\ ratio_{\mathrm{pH8.0}} - AUC\ ratio_{\mathrm{pH5.5}}}$$

As shown in Figure 5, the intensity of 5(6)-FAM increased with increasing pH and a linear correlation was observed from pH 5.5 to pH 8.0 with an R^2 factor of 0.995.

The precision of the sensor was determined by an evaluation function, relating the measured AUC ratio and the pH from the calibration line. As shown in Fig. S5A, the full line represents the evaluation function and the dashed lines indicate the 95% confidence limits of the estimated pH from the curve fitting. By calculating the average variations of the estimated pH's, a mean precision of 0.10 pH units was determined within the operational range from 5.5 to 8.0 (a 300 fold difference in $[H^+]$).[18, 19] The calculated response times t_{90} (the time required to reach 90% of the final equilibrium signal) were 21.6 ± 8.5s and 12.7 ± 0.8s when the buffer solutions were switched from pH 5.5 to 8.0 and from pH 8.0 to 5.5, respectively (Fig. S5B, n=4), significantly shorter than many previously reported optical pH sensors.[18, 41, 42] A decrease in signal (Fig. S5B) with continual laser illumination was observed due to photo-bleaching, an effect that was reduced using a synchronised illumination and measurement regime. Reversibility of the sensor was evaluated in this regime over 5 cycles (pH 5.5 to 8.0 (see Fig. S5C)) with the triggered system with an on demand exposure time of 100 ms during synchronised measurements. Little signal variation was observed during these tests, indicating the robust reversibility of the sensor.

3.5 pH measurement of Lung Cancer Tissue via the Optical-Fibre pH Sensors

An *ex vivo* ovine lung tumour model (Figure 6A) was used to demonstrate the feasibility of the optical fibre pH sensor in/on tissue. This model comprised (half a set of lungs) with both faces of the lung analysed. Three tumorous locations (where the tissue parts were "berry red" and compact) and six healthy locations (where the tissue parts were blush pink and soft) were examined for their pH variation. The optical-fibre pH sensor probe was calibrated, then

inserted through a needle which had been penetrated into the sample locations (Fig. S1C). Each location was analysed with the optical-fibre pH sensor in triplicate, and the mean AUC ratio of each site was calculated. After measurement with the optical-fibre pH sensor, incisions were made within the vicinity (~ 5 mm) of each marked site, followed by measurement with a mini commercial pH meter (Mettler Toledo).

For all nine-sample locations, the pH measured using the optical-fibre pH sensors were found to be in good agreement with the pH measured using the commercial electrode (Figure 6B). From these results, it can also be seen that there is a statistically significant pH difference between healthy and tumorous tissues, suggesting that this hydrogel-based optical fibre pH sensor shows the potential to discriminate between tumorous and normal tissue samples. The data suggested highly local variations in pH tissue environments from healthy to cancerous and shows the robustness of our pH sensor.

4. Conclusions

In this study, we successfully developed a hydrogel based optical fibre pH sensor which allowed ratiometric fluorescence measurements. Using polymer-microarrays a hit polymer (H3) was identified as the optimal immobilization matrix for the pH-indicators for fabrication of the optical fibre pH sensors. Under optimized conditions, the newly developed fibre sensor showed a good linear response to pH within a physiologically relevant pH range between 5.5 and 8.0 with a precision of 0.10 pH units. A rapid response time of 30s was achieved. Finally, this new probe was validated by application in ovine lung cancer tissue.

Due to the important role of real-time pH measurement in numerous endeavors that include industrial, environmental and health monitoring, these hydrogel-based pH sensors have potential applications in areas such as continuous monitoring of blood pH, *in vivo* measurements of gastric pH as well as in construction, for example, measuring pH inside

setting concrete. Additional improvement to the optical fibre probes, such as the use of multi-core fibres, could also result in the development of multi-parameter optical fibre sensors[5] (for pH, O_2, temperature, etc.) based on the hydrogels entrapping multiple sensors. Since sensor construction is based on optical fibres, they have the potential to packaged and used within a variety of scenarios.

CRediT authorship contribution statement

Jingjing Gong: Methodology, Validation, Investigation, Writing – original draft. **Michael G Tanner:** Resources, Writing – Review & Editing. **Seshasailam Venkateswaran:** Conceptualization. **James M Stone:** Resources. **Yichuan Zhang:** Investigation. **Mark Bradley:** Supervision, Writing – Review & Editing, Funding acquisition.

Acknowledgements

Jingjing Gong acknowledges support from the Chinese Scholarship Council and The Henry Lester Trust. We thank the Engineering and Physical Sciences Research Council (UKRI, EPSRC, UK) Interdisciplinary Research Collaboration grants EP/K03197X/1 and EP/R005257/1 for funding. We acknowledge the use of the Cryo FIB/SEM bought with the EPSRC grant EP/P030564/1, Thomas Glen for help with image acquisition, Filip Angelov for tissue preparation, and Wikimedia Commons for the image of lung- simple diagram of lungs and trachea.

Appendix A. Supplementary data

Supplementary material related to this article can be found, in the online version, at doi: XXX

References

[1] J.J. Davenport, M. Hickey, J.P. Phillips, P.A. Kyriacou**,** Dual pO_2/pCO_2 fibre optic sensing film, Analyst., 142 (2017), 1711-1719.

[2] L. Ding, C. Fan, Y. Zhong, T. Li, J. Huang, A sensitive optic fiber sensor based on CdSe QDs fluorophore for nitric oxide detection, Sens. Actuator B: Chem., 185 (2013), 70-76.

[3] A. Deep, U. Tiwari, P. Kumar, V. Mishra, S.C. Jain, N. Singh, P. Kapur, L.M. Bharadwaj, Immobilization of enzyme on long period grating fibers for sensitive glucose detection, Biosens. Bioelectron., 33 (2012), 190-195.

[4] Choudhury, D., Tanner, M.G., McAughtrie, S., Yu, F., Mills, B., Choudhary, T.R., Seth, S., Craven, T.H., Stone, J.M., Mati, I.K., Campbell, C.J., Bradley, M., Williams, C.K., Dhaliwal, K., Birks, T.A., Thomson, R.R.. Endoscopic sensing of alveolar pH. Biomed. Opt. Express., 8, 243-259 (2017).

[5] T.R. Choudhary, M.G. Tanner, A. Megia-Fernandez, K. Harrington, H.A. Wood, A. Marshall, P. Zhu, S.V. Chankeshwara, D. Choudhury, G. Monro, M. Ucuncu, F. Yu, R.R. Duncan, R.R. Thomson, K. Dhaliwal, M. Bradley, High fidelity fibre-based physiological sensing deep in tissue, Sci. Rep., 9 (2019) 1-10.

[6] B.A. Webb, M. Chinenti, M.P. Jacobson, D.L. Barber, Dysregulated pH: a perfect storm for cancer progression, Nat. Rev. Cancer., 11 (2011) 671-677.

[7] M. Chen, C. Chen, Z. Shen, X. Zhang, Y. Chen, F. Lin, X. Ma, C. Zhuang, Y. Mao, H. Gan, P. Chen, X. Zong, R. Wu, Extracellular pH is a biomarker enabling detection of breast cancer and liver cancer using CEST MRI. Oncotarget., 8 (2017) 45759-45767.

[8] K.A. White, B.K. Grillo-Hill, D.L. Barber, Cancer cell behaviors mediated by dysregulated pH dynamics at a glance, J. Cell Sci., 130 (2017) 663-669.

[9] Q. Yang, H. Wang, S. Chen, X. Lan, H. Xiao, H. Shi, Y. Ma, Fiber-optic-based micro-probe using hexagonal 1-in-6 fiber configuration for intracellular Single-Cell pH measurement, Anal. Chem., 87 (2015) 7171-7179.

[10] S. Chen, Q. Yang, H. Xiao, H. Shi, Y. Ma, Local pH monitoring of small cluster of cells using a fiber-optic dual-core micro-probe, Sens. Actuator B: Chem., 241 (2017) 398-405.

[11] J. Wang, Y. Geng, Y. Shen, W. Shi, W. Xu, S. Xu, SERS-active fiber tip for intracellular and extracellular pH sensing in living single cells, Sens. Actuator B: Chem., 290 (2019) 527-534.

[12] E.P. Schartner, M.R. Henderson, M. Purdey, D. Dhatrak, T.M. Monro, P.G. Gill, D.F. Callen, Cancer detection in human tissue samples using a fiber-tip pH probe, Cancer Res., 76 (2016) 6795-6801.

[13] X. Wang, O.S. Wolfbeis, Fiber-optic chemical sensors and biosensors (2015–2019), Anal. Chem., 92 (2020) 397-430.

[14] Q. Cui, O. Podrazký, J. Mrázek, J. Proboštová, I. Kašík, Tapered-fiber optical sensor for physiological pH range, IEEE Sens. J., 15 (2015) 4967-4973.

[15] T.H. Nguyen, T. Venugopalan, S. Tong, K.T.V. Grattan, Intrinsic fiber optic pH sensor for measurement of pH values in the range of 0.5–6, IEEE Sens. J., 16 (2015) 881-887.

[16] F. Mohamad, M.G. Tanner, D. Choudhury, T.R. Choudhary, H.A.C. Wood, K. Harrington, M. Bradley, Controlled core-to-core photo-polymerisation–fabrication of an optical fibre-based pH sensor, Analyst, 142 (2017) 3569-3572.

[17] M. Rosenberg, B.W. Laursen, C.G. Frankær, T.J. Sørensen, A fluorescence intensity ratiometric fiber optics–based chemical sensor for monitoring pH, Adv. Mater. Technol., 3 (2018) 1800205.

[18] C.G. Frankær, K.J. Hussain, T.C. Dörge, T.J. Sørensen, Optical chemical sensor using intensity ratiometric fluorescence signals for fast and reliable pH determination, ACS sens., 4 (2018) 26-31.

[19] T.J. Sørensen, M. Rosenberg, C.G. Frank ær, B.W. Laursen, An optical pH sensor based on diazaoxatriangulenium and isopropyl-bridged diazatriangulenium covalently bound in a composite sol-gel, Adv. Mater. Technol., 4 (2019) 1800561.

[20] H.M.R. Gonçalves, C.D. Maule, P.A.S. Jorge, J.C.G.E Silva, Fiber optic lifetime pH sensing based on ruthenium(II) complexes with dicarboxybipyridine, Anal. Chim. Acta., 626 (2008) 62-70.

[21] S. Islam, R.A. Rahman, Z.B. Othaman, S. Riaz, S. Nassem, Synthesis and characterization of multilayered sol–gel based plastic-clad fiber optic pH sensor, J. Ind. Eng. Chem., 23 (2015) 140-144.

[22] S. Islam, N. Bidin, S. Riaz, G. Krishnan, S. Nassem, Sol–gel based fiber optic pH nanosensor: Structural and sensing properties, Sens. Actuator A: Phys., 238 (2016) 8-18.

[23] S. Islam, H. Bakhtiar, M. S. B. A. Axiz, M. B. Duralim, S. Riaz, S. Nassem, M. B. Abdullha, S. S. Osman, CR incorporation in mesoporous silica matrix for fiber optic pH sensing, Sens. Actuator A: Phys., 280 (2018) 429-436.

[24] S. Islam, H. Bakhtiar, N. Bidin, S. Riaz, S. Nassem, Sol–gel based thermally stable mesoporous TiO_2 nanomatrix for fiber optic pH sensing, J. Sol-Gel Sci. Technol., 86 (2018) 42-50.

[25] S. Islam, H. Bakhtiar, M.B. Duralim, H.H. Jameela, B. Sapingi, S. Riaz, S. Nassem, N.B. Musa, L.P. Suan. M.B. Abdullah, Influence of organic pH dyes on the structural and optical characteristics of silica nanostructured matrix for fiber optic sensing, Sens. Actuator A: Phys., 282 (2018) 28-38.

[26] S. Islam, H. Bakhtiar, S. Nassem, M.S.B.A. Aziz, N. Bidin, S. Riaz, J. Ali, Surface functionality and optical properties impact of phenol red dye on mesoporous silica matrix for fiber optic pH sensing, Sens. Actuator A: Phys., 276 (2018) 267-277.

[27] V. Bhardwaj, A.K. Pathak, V.K. Singh, No-core fiber-based highly sensitive optical fiber pH sensor, J. Biomed. Opt., 22 (2017) 057001.

[28] M.R.R. Khan, , A.V. Watekar, and S. Kang, Fiber-optic biosensor to detect pH and glucose, IEEE Sens. J., 18 (2017) 1528-1538.

[29] S. Derinkuyu, K. Ertekin, O. Oter, S. Denizalti, E. Cetinkaya, Fiber optic pH sensing with long wavelength excitable Schiff bases in the pH range of 7.0-12.0, Anal. Chim. Acta., 588 (2007) 42-49.

[30] C. Chu, C Su, Fluorescence ratiometric optical broad range pH sensor based on CdSe/ZnS quantum dots and O170 embedded in ethyl cellulose matrix, J. Light. Technol., 36 (2018) 857-862.

[31] V. Semwal, B.D. Gupta, Highly sensitive surface plasmon resonance based fiber optic pH sensor utilizing rGO-Pani nanocomposite prepared by in situ method, Sens. Actuator B: Chem., 283 (2019) 632-642.

[32] R. Zhang, A. Liberski, R. Sanchez-Martin, M. Bradley, Microarrays of over 2000 hydrogels–identification of substrates for cellular trapping and thermally triggered release, Biomaterials, 30 (2009) 6193-6201.

[33] C.R. Duffy, R. Zhang, S.-E. How, A. Lilienkampf, P.A. De Sousa, M. Bradley, Long term mesenchymal stem cell culture on a defined synthetic substrate with enzyme free passaging, Biomaterials, 35 (2014) 5998-6005.

[34] A.L. Hook, D.G. Anderson, R. Langer, P. Williams, M.C. Davies, M.R. Alexander, High throughput methods applied in biomaterial development and discovery, Biomaterials, 31 (2010) 187-198.

[35] F. Khan, R.S. Tare, J.M. Kanczler, R.O. Oreffo, M. Bradley, Strategies for cell manipulation and skeletal tissue engineering using high-throughput polymer blend formulation and microarray techniques, Biomaterials, 31 (2010) 2216-2228.

[36] R. Zhang, H.K. Mjoseng, M.A. Hoeve, N.G. Bauer, S. Pells, R. Besseling, S. Velugotla, G. Tourniaire, R.E.B. Kishen, Y. Tsenkina, C. Armit, C.R.E. Duffy, M. Helfen, F. Edenhofer, P.A.D Sousa, M. Bradley, A thermoresponsive and chemically defined hydrogel for long-term culture of human embryonic stem cells, Nat. commun., 4 (2013) 1335-1344.

[37] A.Hansen, H.K. Mjoseng, R.Zhang, M. Kalloudis, V. Koutsos, P.A. de Sousa, M. Bradley**,** High-density polymer microarrays: Identifying synthetic polymers that control human embryonic stem cell growth, Adv. Healthcare Mater., 3 (2014), 848-853.

[38] A. Liberski, R.Zhang, M. Bradley, Inkjet fabrication of polymer microarrays and grids-solving the evaporation problem, Chem. Commun., 3 (2009), 334-336.

[39] A.Hansen, R.Zhang, M. Bradley**,** Fabrication of arrays of polymer gradients using inkjet printing, Macromol. Rapid Commun., 33 (2012), 1114-1118.

[40] J. Gong, S. Venkateswaran, M. G. Tanner, J. M. Stone, M. Bradley, Polymer microarrays for the discovery and optimization of robust optical-fiber-based pH sensors, ACS Comb. Sci., 21 (2019) 417-424.

[41] M. Yin, M. Yao, S. Gao, A. P. Zhang, H. Tam, P. A. Wai, Rapid 3D patterning of poly (acrylic acid) ionic hydrogel for miniature pH sensors, Adv. Mater., 28 (2016) 1394-1399.

[42] P.J. Rivero, J. Goicoechea, M. Hernaez, A. B. Socorro, I. R. Matias, F. J. Arregui, Optical fiber resonance-based pH sensors using gold nanoparticles into polymeric layer-by-layer coatings, Microsyst. Technol., 22 (2016) 1821-1829.

Figure captures:

Figure 1. The polymer microarray approach used to identify lead polymers for dye trapping and pH sensing. (A) Hydrogel microarray inkjet fabrication process. (B) The separation between the polymer features. (C) Fluorescence images for the polymer microarray after incubation in pH 10.0 and pH 4.0 buffers, respectively.

Figure 2. (A) Preparation of the optical fibre sensor. (B) Structure of the hit polymer (H3).

Figure 3. Fold increase in fluorescence for the top eight polymers identified from scale-up (hydrogels polymerised onto glass cover slips). Error bars represent the standard deviation in the variation of fold increase in intensity from three polymer-coated coverslips between pH 4.0 and pH 10.0.

Figure 4. (A-C) SEM images of fibre tip. (D-F) Images of the distal surface of the coated optical fibre under white light and fluorescence (excitation: 485/20 nm, emission: 530/20 nm and excitation: 628/40 nm, emission: 692/40) microscopy. (G-H) Side images of the tip of optical fibre pH probe before and after pH measurement under fluorescence microscopy (excitation: 485/20 nm, emission: 530/20 nm).

Figure 5. (A) Emission spectra of the hydrogel-based optical fibre pH sensors. (B) Calibration lines of the hydrogel-based optical fibre pH sensors between pH 5.5 to 8.0 (normalized to the interval of [0,1]). Note: Although the intensity linearity of 5(6)-FAM showed a slight deviation (Figure 5A) the AUC ratios for the two dyes showed good linearity as the Porphyrin intensity exhibited slight changes with increasing pH.

Figure 6. (A) Photograph of lung tissue, with the probe sampling locations marked on the image. (B) The pH measured using the optical fibre sensor (x-axis). The y-axis represents the pH measured using the commercial glass-electrode pH meter. The X and Y error bars represent the standard deviations over three replicate measurements for both the optical fibre sensor (X), and the commercial glass-electrode pH meter (Y).

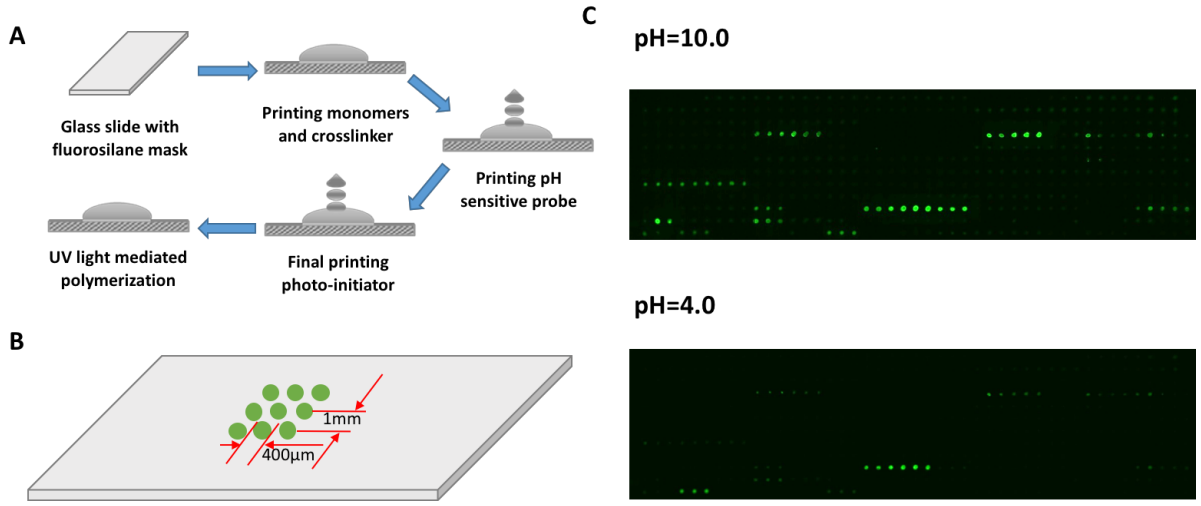

Figure 1. The polymer microarray approach used to identify lead polymers for dye trapping and pH sensing. (A) Hydrogel microarray inkjet fabrication process. (B) The separation between the polymer features. (C) Fluorescence images for the polymer microarray after incubation in pH 10.0 and pH 4.0 buffers, respectively.

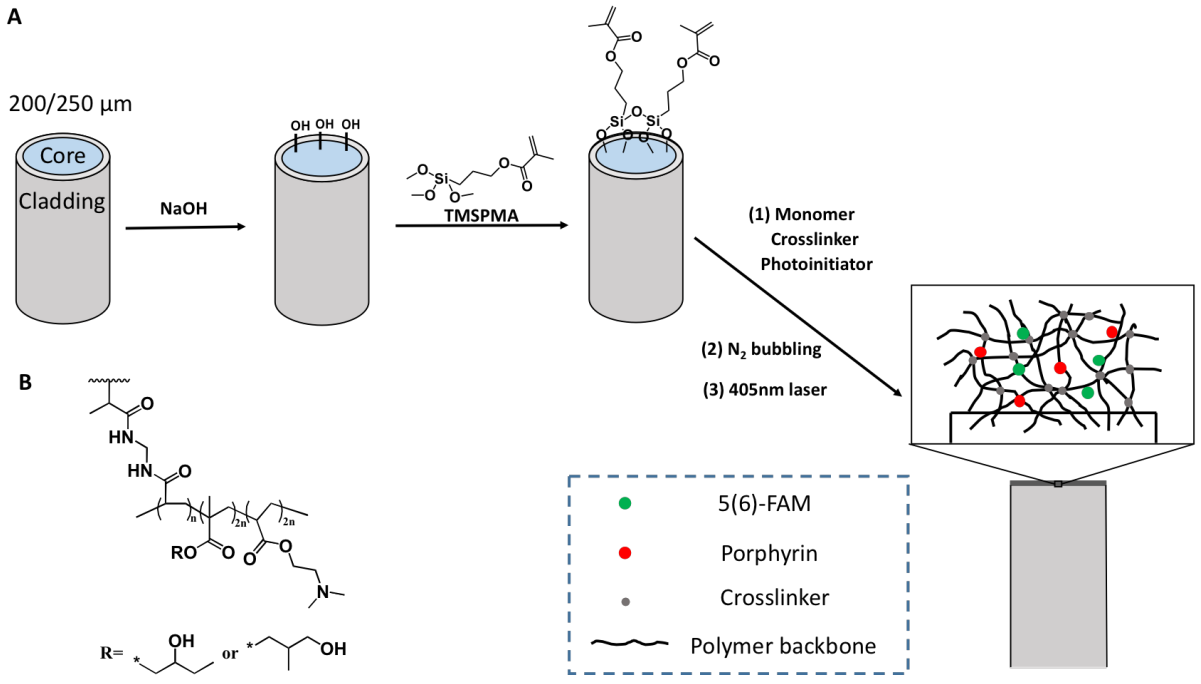

Figure 2. (A) Preparation of the optical fibre sensor. (B) Structure of the hit polymer (H3).

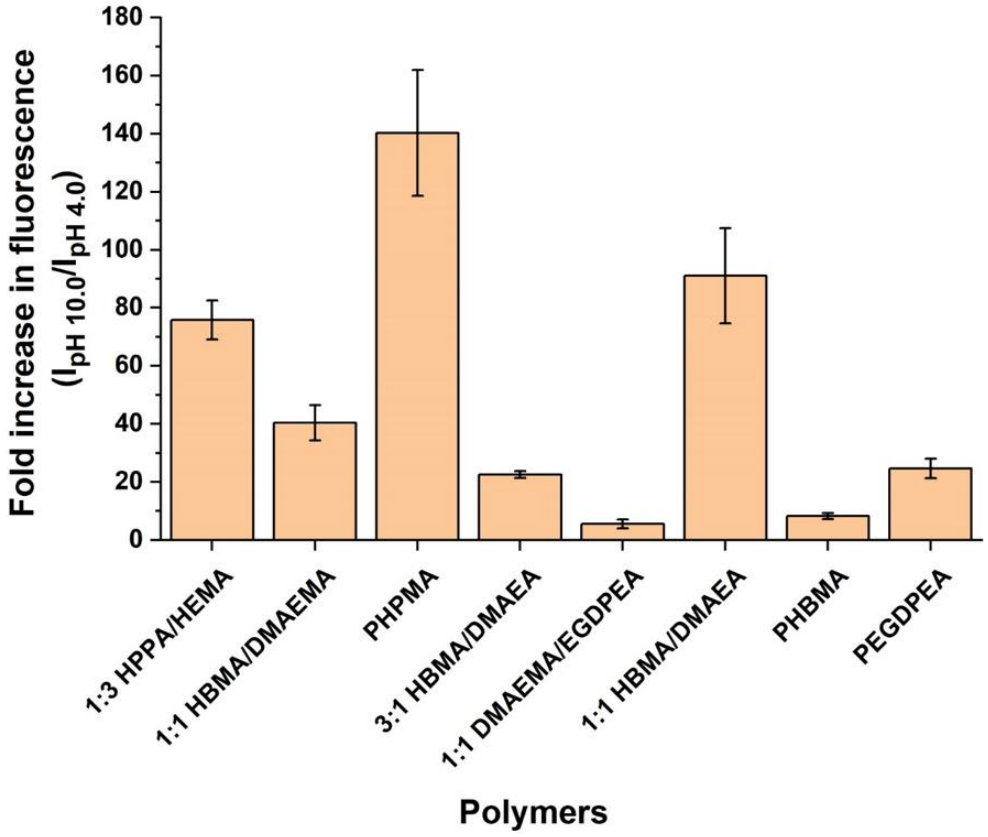

Figure 3. Fold increase in fluorescence for the top eight polymers identified from scale-up (hydrogels polymerised onto glass cover slips). Error bars represent the standard deviation in the variation of fold increase in intensity from three polymer-coated coverslips between pH 4.0 and pH 10.0.

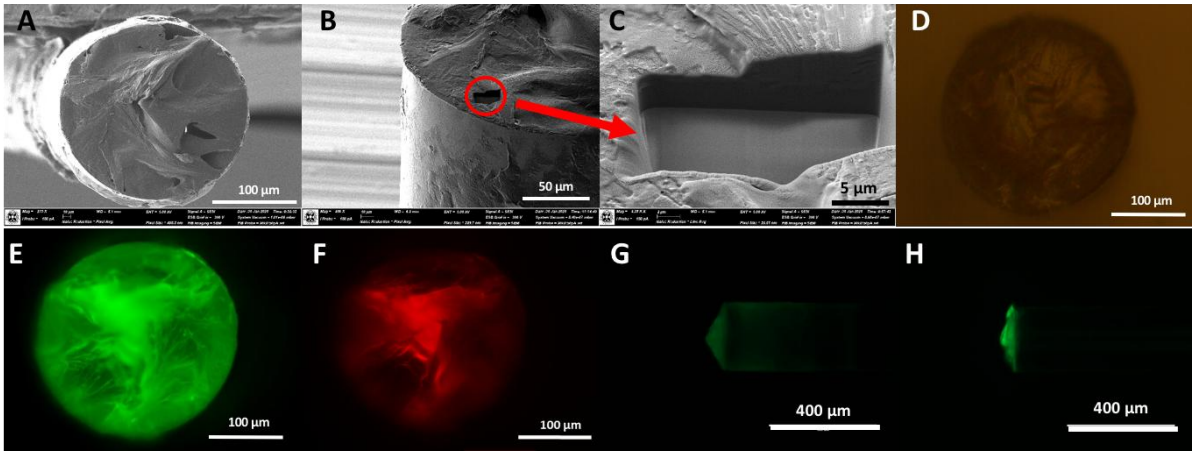

Figure 4. (A-C) SEM images of fibre tip. (D-F) Images of the distal surface of the coated optical fibre under white light and fluorescence (excitation: 485/20 nm, emission: 530/20 nm and excitation: 628/40 nm, emission: 692/40) microscopy. (G-H) Side images of the tip of optical fibre pH probe before and after pH measurement under fluorescence microscopy (excitation: 485/20 nm, emission: 530/20 nm).

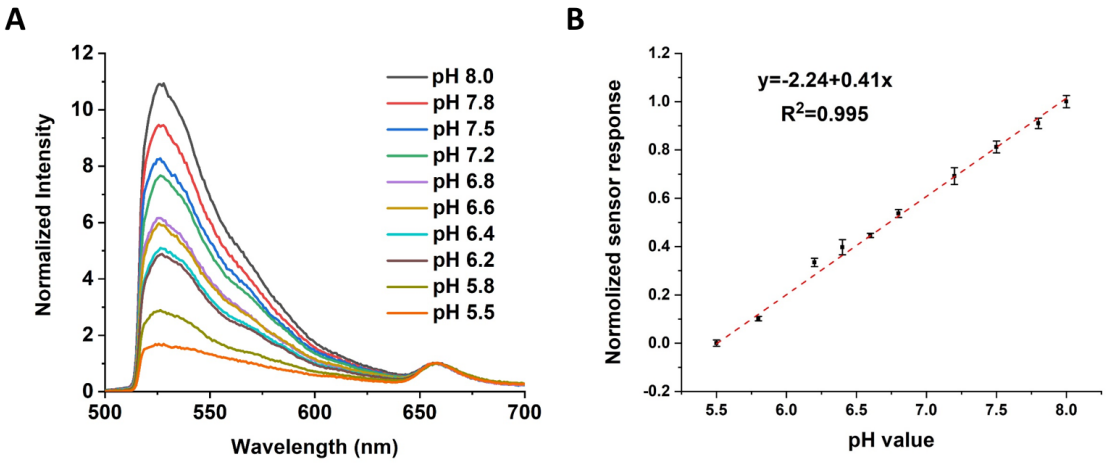

Figure 5. (A) Emission spectra of the hydrogel-based optical fibre pH sensors. (B) Calibration lines of the hydrogel-based optical fibre pH sensors between pH 5.5 to 8.0 (normalized to the interval of [0,1]). Note: Although the intensity linearity of 5(6)-FAM

showed a slight deviation (Figure 5A) the AUC ratios for the two dyes showed good linearity as the Porphyrin intensity exhibited slight changes with increasing pH.

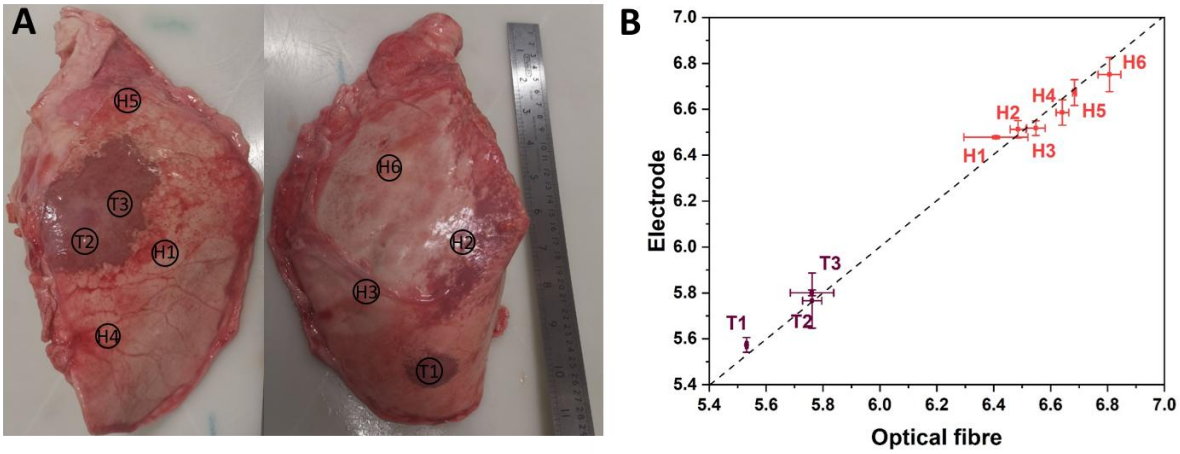

Figure 6. (A) Photograph of lung tissue, with the probe sampling locations marked on the image. (B) The pH measured using the optical fibre sensor (x-axis). The y-axis represents the pH measured using the commercial glass-electrode pH meter. The X and Y error bars represent the standard deviations over three replicate measurements for both the optical fibre sensor (X), and the commercial glass-electrode pH meter (Y).